NANO LETTERS

pubs.acs.org/NanoLett
Letter

Nanoscale Tracking of the High-Temperature Spin-State Transition in $LaCoO_3$

Michelle A. Smeaton,* Elena Salagre, Elliot J. Fuller, Lance M. Wheeler, and Katherine L. Jungjohann*

Cite This: *Nano Lett.* 2025, 25, 16340−16345

ABSTRACT: The high-temperature spin and electronic transitions in $LaCoO_3$ have recently been leveraged to create neuromorphic (brain-inspired) devices. While these devices have shown the potential for impactful functionality in next-generation computing systems, the nanoscale dynamics of the spin and electronic transitions that underlie their operation are not well understood. Inhomogeneities related to interfaces, electrode contacts, strain, and crystal defects can all affect device performance, making nanoscale characterization of the transitions essential for producing consistent and reliable devices. Here, we demonstrate the first nanoscale in situ measurement of the spin transition in $LaCoO_3$ at device-relevant temperatures (25−325 °C) over length scales of tens of nanometers using STEM-EELS. This measurement is enabled by an Al_2O_3 coating, which prevents unwanted reduction of the $LaCoO_3$ specimen at high temperature and vacuum. The detailed understanding of $LaCoO_3$ transition dynamics enabled by such measurements will be crucial for optimizing $LaCoO_3$-based neuromorphic devices and increasing reliability for real-world application.

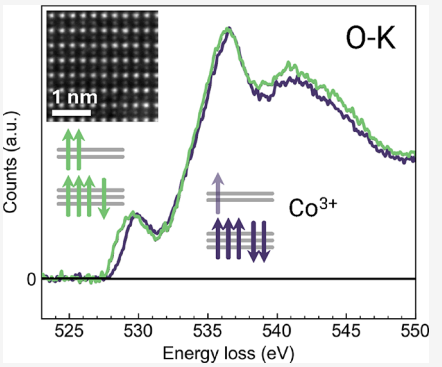

KEYWORDS: *$LaCoO_3$, STEM, EELS, in situ, complex oxides, spin transition*

Lanthanum cobalt oxide ($LaCoO_3$) has garnered significant research attention over the last several decades due to its strongly correlated nature, which gives rise to intriguing electronic and magnetic properties.[1−4] While $LaCoO_3$ has historically been used in solid oxide fuel cell cathodes[5,6] and catalysis,[7,8] interest has grown in its use for advanced microelectronics applications, including brain-inspired (neuromorphic) computing.[9−14] For example, the broad, above-room-temperature electronic transition exhibited by $LaCoO_3$ has recently been leveraged to demonstrate biological axon-like active signal transmission in an adjacent conductor.[12] The discovery enables electrical signal amplification without breaking the conductor to introduce additional amplifiers in the circuit. Breakthroughs like this justify pursuing the nanoscale integration of materials like $LaCoO_3$ into the next development phase of neuromorphic computing devices.

Though $LaCoO_3$ has shown promise as a switchable electronic material, the physics underlying the spin and electronic transitions in $LaCoO_3$ are still not fully understood, limiting material development and opportunity for implementation in reliable, nanoscale neuromorphic devices. It is accepted that the interplay between spin, electronic, and lattice degrees of freedom in $LaCoO_3$ leads to a spin transition at low temperature (~90 K) and a broad semiconductor-to-metal transition (SMT) above room temperature (~300−600 K), which is concomitant with a further broad spin transition.[15−17] This complexity arises from the Co ion, which has a nominal formal charge of 3+ and thus a partially filled 3*d* band. Comparable values for the interatomic exchange energy (J_H) and crystal field splitting (10 Dq) between the e_g and t_{2g} states in $LaCoO_3$ mean that the possible spin states are very close in energy (Figure 1a). The preferred state is thus sensitively dependent on the precise crystal field magnitude, which is a function of Co−O bond length and O−Co−O bond angle.[18,19]

In the case of electrothermal oscillator devices used in artificial neurons or axons, which make use of the high temperature SMT and spin transition, the situation is even more complex.[12] Such nanoscale devices are expected to contain inhomogeneities due to strain, contacting electrodes, and crystal defects, which affect their function. Thus, nanoscale characterization techniques are required to understand the connections among the processing, structure, and ultimate properties of devices. X-ray and neutron scattering methods have been used extensively to study the averaged microscale structural and chemical changes characteristic of the high temperature transitions in $LaCoO_3$.[2,4,20,21] However, the spatial resolutions of these techniques lead to averaging over areas larger than the expected heterogeneities in nanoscale devices, meaning that crucial details could be obscured. When

Received: July 26, 2025
Revised: October 25, 2025
Accepted: October 28, 2025
Published: November 5, 2025

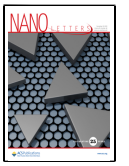

https://doi.org/10.1021/acs.nanolett.5c03863
Nano Lett. 2025, 25, 16340−16345

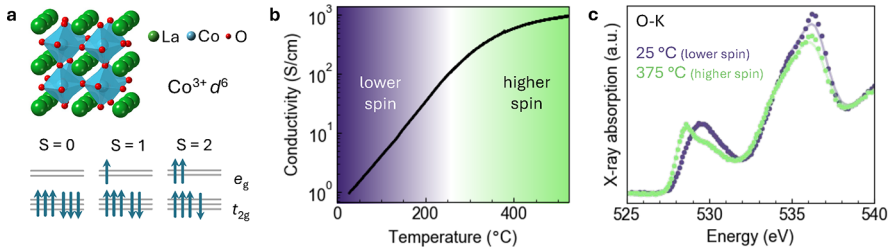

Figure 1. Macroscale structure and electronic properties of $LaCoO_3$ thin films. (a) Atomic model of $LaCoO_3$ and energy level diagrams for the Co^{3+} ion in the low, intermediate, and high spin states. (b) Temperature-dependent electrical conductivity data showing a broad insulator-to-metal transition between room temperature and 500 °C. (c) X-ray absorption spectroscopy (XAS) O−K edge spectra acquired at room temperature and 375 °C from the same film measured in b, which exhibits a clear shift in the prepeak feature (~530 eV) toward lower energy at high temperature. The data in c was adapted from ref 13. Available under a CC-BY 4.0 license. Copyright 2024 Woo et al.

the material is scaled down for such devices, larger-scale probes are unable to capture the effects of interfaces or nanoscopic defects, which can have outsized effects at such small scales. To effectively implement electrical oscillator devices in next-generation computing technology, we need to be able to track and evaluate the spin-state transition in devices at the nanoscale, necessitating nanoscale characterization techniques.

While controversy remains over the exact states associated with the low- and high-temperature transitions, one common interpretation holds that the Co^{3+} ions occupy a mix of three different states (Figure 1a): a low spin state (t_{2g}^6, S = 0), an intermediate spin state ($t_{2g}^5\ e_g^1$, S = 1), and a high spin state ($t_{2g}^4\ e_g^2$, S = 2), with the proportion of Co^{3+} ions in each state changing with each observed transition.[3,22] More complex spin states have also been suggested.[23,24] Nonetheless, the changing spin states have been reported to produce distinct signatures in the near-edge fine structure of the O−K edge as measured by spectroscopic methods such as X-ray absorption spectroscopy (XAS)[2,13] and electron energy loss spectroscopy (EELS).[25]

EELS in scanning transmission electron microscopy (STEM) has significant potential for analyzing complex electronic transitions in correlated oxides. It can achieve sub-Angstrom spatial resolution, with energy resolution similar to that attainable by XAS.[26,27] In situ temperature-controlled STEM experiments enable high-temperature spectroscopic and structural measurements with nano- to atomic-scale spatial resolution.[28,29] However, the instability of $LaCoO_3$ in reducing environments (such as the high vacuum of the STEM sample region)[30] have so far prevented in situ STEM characterization of the high-temperature transitions in $LaCoO_3$. Though the low-temperature spin transition in $LaCoO_3$ has been previously measured at the nanoscale by STEM-EELS,[25] the high temperature transition has not.

Here, we leverage the combined spatial and energy resolution of STEM-EELS to measure the spin-state transition in $LaCoO_3$ between room temperature and ~300 °C over a total field of view of ~90 nm × 90 nm. The measurement was enabled by a method to conformally coat $LaCoO_3$ STEM specimens, creating an effective barrier to oxygen loss during heating under high vacuum. The ability to measure the $LaCoO_3$ spin state at the nanoscale will enable the characterization of local heterogeneity in the state transition, including in devices currently under investigation for neuromorphic computing applications. Detailed understanding of transition dynamics will be crucial for developing these devices to be consistent and reliable.

$LaCoO_3$ thin films and freestanding $LaCoO_3$ flakes were grown by using pulsed laser deposition (PLD) on $LaAlO_3$(100) substrates (see Supporting Information for growth details). Raman, X-ray photoelectron spectroscopy, and X-ray Diffraction and Reflectivity data were acquired to determine film quality and thickness (see Supporting Information Figure S1). The $LaCoO_3$ thin films exhibit the expected broad SMT as a function of temperature above 25 °C (Figure 1b). As previously reported for these $LaCoO_3$ films, XAS O−K edge spectra acquired at room temperature and 375 °C exhibit a clear shift in the prepeak feature at ~530 eV (Figure 1c).[13] This result is consistent with earlier studies based on bulk $LaCoO_3$, which attribute it to the low-to-high spin-state transition.[2] While this provides clear evidence of the spin-state transition in these thin films, XAS cannot provide sufficient spatial resolution to investigate the effects of local heterogeneity on the transition, which in turn influences the operation of oscillator devices of interest for neuromorphic applications. These heterogeneities are expected to occur on the scale of Angstroms to hundreds of nanometers, well below the spot size of X-ray sources. STEM-EELS measurements can be performed with down to sub-Angstrom resolution and probe nominally the same electronic transitions as validated by XAS.

$LaCoO_3$ TEM samples were prepared on commercial microelectro-mechanical system (MEMS) heating chips in two geometries: focused ion beam (FIB) lamellas (Figure 2a−c) and freestanding flakes (Figure 2d−f) (see Supporting Information for sample preparation and STEM imaging details). Figure 2 presents an overview of these sample geometries as imaged by scanning electron microscopy (SEM) and STEM. The cross-sectional lamella samples exhibit an ~5 nm epitaxial layer at the substrate interface, above which the film relaxes via the formation of misfit dislocations (Figure 2c). The dislocations are also clearly visible in the plane-view flake samples (Figure 2f), where they appear to form a random network of vertical and horizontal line defects. A few of the line defects are indicated with arrows in the same image reproduced in Supporting Information Figure S2. While the abundance of these dislocations was not found to suppress the spin and insulator-to-metal transitions, they may affect the temperature range and dynamics of these transitions.

For STEM in situ heating experiments, prepared $LaCoO_3$ samples were coated with a ~10 nm layer of amorphous Al_2O_3 using atomic layer deposition (ALD) to form a conformal layer (Figure 2g, see Supporting Information for deposition details). This coating prevents the loss of oxygen from the $LaCoO_3$ during heating due to the reducing environment created by the high-vacuum of the STEM column. At the same time, the low Z number of the constituent elements and the amorphous

https://doi.org/10.1021/acs.nanolett.5c03863
Nano Lett. 2025, 25, 16340−16345

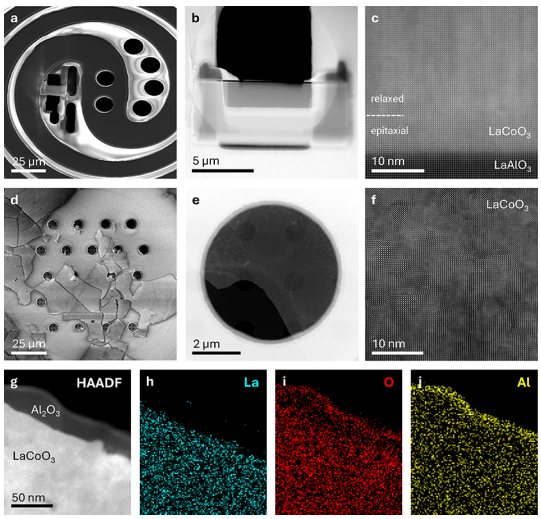

Figure 2. $LaCoO_3$ scanning transmission electron microscopy (STEM) sample preparation. (a–c) Scanning electron microscopy (SEM) (a) and high-angle annular dark-field (HAADF)-STEM (b,c) images of a focused ion beam (FIB) lamella placed on an in situ heating chip for a TEM heating holder. Epitaxially strained and relaxed layers of the $LaCoO_3$ film are labeled in c. (d–f) SEM (d) and HAADF-STEM (e,f) images of freestanding flakes mechanically transferred to an in situ heating chip for a TEM heating-biasing holder. (g–j) Simultaneously acquired HAADF-STEM image (g) and energy dispersive X-ray spectroscopy (EDS) elemental maps (h–j) for La, O, and Al, respectively, showing a continuous ~15 nm Al_2O_3 coating extending over the edge of a flake.

nature of the film prevent it from contributing significant contrast to the STEM images. The coating thickness was chosen to balance effective barrier properties with deterioration of STEM-EELS data. Ten nm was estimated to be well above a minimum thickness for blocking oxygen loss based on previous studies of oxygen diffusion in amorphous ALD Al_2O_3,[31] and we found it did not noticeably degrade the clarity of the EELS O–K prepeak analyzed herein. The consistency and thickness of the Al_2O_3 coating was confirmed using STEM energy dispersive X-ray spectroscopy (EDS) as shown in Figure 2g–j. To the best of our knowledge, this is the first reported use of Al_2O_3 as a barrier to sample evolution during S/TEM analysis.

Initially, amorphous carbon was employed as a barrier coating (see Supporting Information Figure S3), as it was previously shown to prevent ion diffusion during STEM imaging of beam-sensitive metal halide perovskite materials.[32] However, amorphous carbon did not suppress oxygen loss sufficiently for the measurement of the $LaCoO_3$ spin-state transition. This is perhaps due to inadequate density of the thermally evaporated carbon. Graphene has also been employed as an encapsulation layer to prevent sample damage during TEM imaging.[33] This method would be highly challenging in the present case, however, due to the geometry of the $LaCoO_3$ samples and the underlying MEMS heating chips. Therefore, ALD coating was pursued, as it is well-understood to produce reliable, thin, and pinhole free coatings.

EELS O–K edge spectra of an Al_2O_3-coated $LaCoO_3$ flake sample acquired at 25 and 300 °C over tens of nanometer fields of view (Figure 3a) show a distinct shift in the prepeak feature (peak i) toward lower energy at elevated temperature. This prepeak is well-understood to represent hybridization between the O 2*p* and transition metal (Co) 3*d* orbitals,[34] while peaks ii and iii are commonly attributed to hybridization with the A site (La) 5*d* and transition metal (Co) 4*sp* orbitals, respectively.[2] Here, a shift in the prepeak (peak i) to lower energy indicates an increase in available lower energy t_{2g} orbitals, as electron density shifts to the higher energy e_g orbitals due to the spin-state transition. Note that the prepeak feature is not affected by the O–K edge signal from the Al_2O_3 coating, as the onset of that signal occurs at ~533 eV (see Supporting Information Figure S4a). Thus, the alumina only contributes to an intensity increase and broadening of peaks ii and iii from ~533–545 eV, which are not used in this analysis. Additionally, O–K edge spectra were acquired before and after Al_2O_3 coating and their features compared to ensure that the coating process did not cause appreciable reduction of the $LaCoO_3$ samples prior to in situ experiments (see Supporting Information Figure S4).

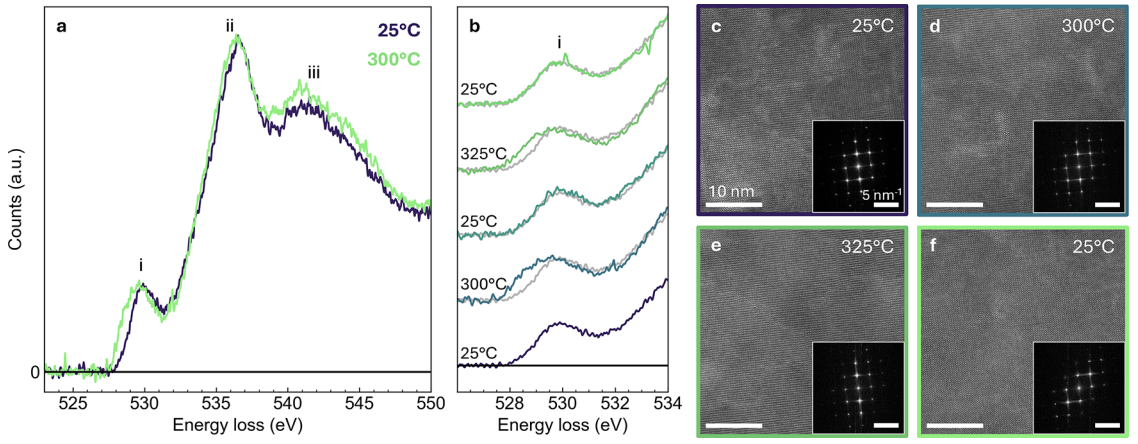

Figure 3. In situ STEM electron energy loss spectroscopy (EELS) measurement of the $LaCoO_3$ spin transition. (a) O–K edge EEL spectra of an Al_2O_3 coated $LaCoO_3$ flake acquired at 25 and 300 °C. The prepeak feature (labeled (i)) exhibits a clear shift to lower energy at elevated temperature, indicating a transition to a higher spin state. (b) Prepeak region of the O–K edge acquired during two heating cycles between 25 and 300–325 °C, showing that the shift in the prepeak feature is reversible and repeatable. The initial 25 °C spectrum is repeated in gray with each subsequent spectrum for ease of comparison. (c–f) HAADF-STEM images acquired during in situ heating at 25, 300, and 325 °C and back to 25 °C, respectively, showing no observable changes in structure. The fast Fourier transform (FFT) of each image is included as an inset.

https://doi.org/10.1021/acs.nanolett.5c03863
Nano Lett. 2025, 25, 16340–16345

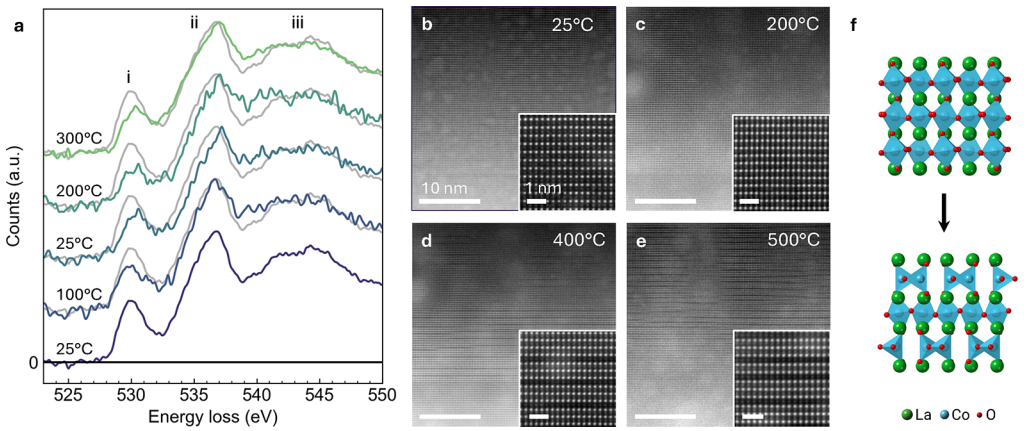

Figure 4. In situ heating of uncoated $LaCoO_3$ cross-sectional FIB lamella. (a) O−K edge EEL spectra of the uncoated $LaCoO_3$ acquired during two heating cycles, exhibiting irreversible changes to the prepeak feature (labeled (i)) after heating to only 100 °C. The initial 25 °C spectrum is repeated with each subsequent spectrum for ease of comparison. (b−e) HAADF-STEM images acquired during heating at 25, 200, 400, and 500 °C, respectively, showing the formation and increasing frequency of dark horizontal lines, indicative of ordered oxygen vacancies. The insets show a magnified field of view for each temperature. Low-frequency intensity variation is due to residual tungsten from FIB lamella preparation on the sample surface. (f) Atomic models representing the transition from the perovskite ($LaCoO_3$) to brownmillerite ($LaCoO_{2.5}$) structure upon loss of oxygen from the sample.

EELS O−K edge measurements were repeated for two heating cycles between 25 and 300−325 °C (Figure 3b, see Supporting Information Figure S5 for full spectra). During cycling, the shift in the prepeak feature at high-temperature is fully reversible. Each subsequent spectrum acquired at room temperature matches the initial spectrum (repeated in gray for ease of comparison). Additionally, the shift is repeatable, showing the same behavior for the two high-temperature cycles. We can, therefore, be confident that there are no unintended irreversible changes to the sample during heating and that the prepeak shift is due to the reversible spin-state transition. We note that heating the sample further to 375 °C does begin to cause irreversible reduction of the film (see Supporting Information Figure S6), which suppresses the spin transition. We discuss this reduction process in detail below.

HADDF-STEM images (Figure 3c−f) show no observable changes to the atomic structure of the $LaCoO_3$ flake. All images show a random distribution of dislocations, which do not notably evolve at the studied temperatures. Furthermore, fast Fourier transforms (FFTs) of the images (Figure 3c−f insets) show no change in crystal symmetry, though there may be slight changes to the extent of tilting in the CoO_6 octahedra that are not resolvable here. These observations are consistent with previous studies reporting the only structural change accompanying the spin-state transition to be a decrease in the rhombohedral distortion of the $LaCoO_3$ unit cell.[35] While measurement of the oxygen octahedral tilts comprising the rhombohedral distortion of the perovskite unit cell is possible, it would require a very precise visualization of the oxygen anions. Such measurements are extremely challenging, even with the double-tilt TEM holder capability necessary to reach the precise crystalline zone-axis. The lack of structural changes noted here also supports the lack of any unintended reactions, such as reduction, that could occur during the experiment.

Overall, the EELS and structural characterization described herein are consistent with previous X-ray scattering measurements of the high-temperature spin transition.[2,13] The present measurement technique enables future direct tracking of the spin transition across nanoscale features such as those likely present in electrothermal oscillator devices for neuromorphic computing.[12] This type of characterization will be critical for optimizing device function and increasing consistency and reliability for real-world implementation.

In situ STEM measurements performed on $LaCoO_3$ without an Al_2O_3 coating, revealed significant reduction of $LaCoO_3$ upon heating (Figure 4). This reduction suppresses the spin transition and thus prevents its measurement. Heating a FIB lamella to just 100 °C and cooling back to room temperature reveals irreversible reduction of the $LaCoO_3$ (Figure 4a), as evidenced by the decrease in prepeak (peak i) intensity in the spectrum obtained at 25 °C after cooling as compared to the spectrum acquired prior to any heating (repeated in light gray for ease of comparison). This reduction continues when the temperature is raised incrementally to 200 and then 300 °C, with the prepeak intensity decreasing progressively with the oxygen content.

Whereas HAADF-STEM imaging initially shows no change in the atomic structure of the uncoated specimen, it reveals dark lines beginning to form in the $LaCoO_3$ lattice when heated to 400 °C (Figure 4b−e). These lines form in CoO_2 layers starting at random intervals before forming in approximately every third layer and finally every second layer. The dark lines are caused by ordered oxygen vacancies in those layers. Ordering in every other CoO_2 layer is characteristic of the brownmillerite ($LaCoO_{2.5}$) structure. This transition from the perovskite to an intermediate and then the brownmillerite structure in $LaCoO_{3-\delta}$ (Figure 4f) has previously been observed using electron beam-induced reduction in the STEM[36] and is consistent with phase behavior in bulk $LaCoO_{3-\delta}$.[37] To the best of our knowledge, it has not been previously demonstrated by in situ heating. This data also conclusively shows that the dark lines observed in CoO_2 layers of $LaCoO_3$ arise from oxygen vacancy formation, not the spin-state transition, as has previously been suggested.[38,39]

In summary, we have demonstrated in situ measurement of the high-temperature spin-state transition in $LaCoO_3$ over length scales of just tens of nanometers. The ability to track the spin transition over these length scales enables characterization of the effects of nanostructure and local heterogeneity on the spin-state transition and concomitant SMT, as well as the

https://doi.org/10.1021/acs.nanolett.5c03863
Nano Lett. 2025, 25, 16340−16345

dynamics underlying electrical oscillations central to neuromorphic devices like those demonstrated by Brown et al.[12] These measurements were enabled by a method to prevent reduction of STEM specimens during in situ heating by coating them with a thin, conformal layer of alumina deposited by ALD. This pinhole free, conformal coating ensured oxygen could not escape the specimen during heating in the high vacuum of the STEM column and allowed for EELS measurement of the O−K edge up to 325 °C. The ability to make these measurements with nanoscale spatial resolution and high energy resolution represents an important step toward understanding the structure−property relationships underpinning the function of electrical oscillator devices and therefore optimizing their performance. The coating method developed here also offers a method to protect other sensitive specimens (oxides and otherwise) from reduction during in situ high-temperature STEM characterization.

■ ASSOCIATED CONTENT

Data Availability Statement

The data that support the findings of this study are available from the corresponding author upon reasonable request.

Supporting Information

The Supporting Information is available free of charge at https://pubs.acs.org/doi/10.1021/acs.nanolett.5c03863.

Sample growth and STEM experimental details, film characterization, additional STEM imaging and EELS data for carbon- and Al_2O_3-coated samples (PDF)

■ AUTHOR INFORMATION

Corresponding Authors

Michelle A. Smeaton − *Materials Science Center, National Renewable Energy Laboratory, Golden, Colorado 80401, United States;* orcid.org/0000-0001-9114-1009; Email: michelle.smeaton@nrel.gov

Katherine L. Jungjohann − *Materials Science Center, National Renewable Energy Laboratory, Golden, Colorado 80401, United States;* orcid.org/0000-0002-8132-1230; Email: katherine.jungjohann@nrel.gov

Authors

Elena Salagre − *Materials Physics Department, Sandia National Laboratories, Livermore, California 94550, United States*

Elliot J. Fuller − *Materials Physics Department, Sandia National Laboratories, Livermore, California 94550, United States;* orcid.org/0000-0001-7912-8688

Lance M. Wheeler − *Materials Science Center, National Renewable Energy Laboratory, Golden, Colorado 80401, United States;* orcid.org/0000-0002-1685-8242

Complete contact information is available at: https://pubs.acs.org/10.1021/acs.nanolett.5c03863

Notes

The authors declare no competing financial interest.

■ ACKNOWLEDGMENTS

This work was authored, in part, by the National Renewable Energy Laboratory (NREL) for the U.S. Department of Energy (DOE) under Contract No. DE-AC36-08GO28308. The growth and bulk characterization at Sandia National Laboratories and the sample preparation and STEM characterization of coated samples at NREL were supported as part of the Reconfigurable Materials Inspired by Nonlinear Neuron Dynamics (reMIND) Energy Frontier Research Center funded by the U.S. DOE, Office of Science, Basic Energy Sciences. STEM characterization of the uncoated sample made use of the electron microscopy facility of the Platform for the Accelerated Realization, Analysis, and Discovery of Interface Materials (PARADIM), which is supported by the National Science Foundation under Cooperative Agreement No. DMR-2039380. The views expressed in the article do not necessarily represent the views of the DOE or the U.S. Government. The U.S. Government retains and the publisher, by accepting the article for publication, acknowledges that the U.S. Government retains a nonexclusive, paid-up, irrevocable, worldwide license to publish or reproduce the published form of this work, or allow others to do so, for U.S. Government purposes.

■ REFERENCES

(1) Raccah, P. M.; Goodenough, J. B. First-Order Localized-Electron ↔ Collective-Electron Transition in $LaCoO_3$. *Phys. Rev.* **1967**, *155*, 932−943.

(2) Abbate, M.; Fuggle, J. C.; Fujimori, A.; Tjeng, L. H.; Chen, C. T.; Potze, R.; Sawatzky, G. A.; Eisaki, H.; Uchida, S. Electronic structure and spin-state transition of $LaCoO_3$. *Phys. Rev. B* **1993**, *47*, 16124−16130.

(3) Korotin, M. A.; Ezhov, S. Y.; Solovyev, I. V.; Anisimov, V. I.; Khomskii, D. I.; Sawatzky, G. A. Intermediate-spin state and properties of LaCoO 3. *Phys. Rev. B* **1996**, *54*, 5309−5316.

(4) Haverkort, M. W.; Hu, Z.; Cezar, J. C.; Burnus, T.; Hartmann, H.; Reuther, M.; Zobel, C.; Lorenz, T.; Tanaka, A.; Brookes, N. B.; Hsieh, H. H.; Lin, H.-J.; Chen, C. T.; Tjeng, L. H. Spin State Transition in $LaCoO_3$ Studied Using Soft X-ray Absorption Spectroscopy and Magnetic Circular Dichroism. *Phys. Rev. Lett.* **2006**, *97*, 176405.

(5) Huang, K.; Lee, H. Y.; Goodenough, J. B. Sr- and Ni-Doped LaCoO3 and LaFeO3 Perovskites: New Cathode Materials for Solid-Oxide Fuel Cells. *J. Electrochem. Soc.* **1998**, *145*, 3220.

(6) Sun, C.; Hui, R.; Roller, J. Cathode materials for solid oxide fuel cells: a review. *J. Solid State Electrochem.* **2010**, *14*, 1125−1144.

(7) Voorhoeve, R. J. H.; Johnson, D. W.; Remeika, J. P.; Gallagher, P. K. Perovskite Oxides: Materials Science in Catalysis. *Science* **1977**, *195*, 827−833.

(8) Zhu, H.; Zhang, P.; Dai, S. Recent Advances of Lanthanum-Based Perovskite Oxides for Catalysis. *ACS Catal.* **2015**, *5*, 6370−6385.

(9) Zhang, S.; Galli, G. Understanding the metal-to-insulator transition in $La_{1x}Sr_xCoO_3$ and its applications for neuromorphic computing. *npj Computational Materials* **2020**, *6*, 1−9.

(10) Kumar, A.; Kumari, K.; Ray, S. J.; Thakur, A. D. Graphene mediated resistive switching and thermoelectric behavior in lanthanum cobaltate. *J. Appl. Phys.* **2020**, *127*, 235103.

(11) Bhattacharya, R.; Khanna, A.; Bosworth, B.; Orloff, N.; Gambin, V.; Streit, D.; Fay, P.; Datta, S. Thermally Resilient Microwave Switch and Power Limiter based on Insulator-Metal Transition of Lanthanum Cobalt Oxide. In *2022 International Electron Devices Meeting (IEDM)*, 2022; pp 70−73.

(12) Brown, T. D.; Zhang, A.; Nitta, F. U.; Grant, E. D.; Chong, J. L.; Zhu, J.; Radhakrishnan, S.; Islam, M.; Fuller, E. J.; Talin, A. A.; Shamberger, P. J.; Pop, E.; Williams, R. S.; Kumar, S. Axon-like active signal transmission. *Nature* **2024**, *633*, 804−810.

(13) Woo, K. S.; Zhang, A.; Arabelo, A.; Brown, T. D.; Park, M.; Talin, A. A.; Fuller, E. J.; Bisht, R. S.; Qian, X.; Arroyave, R.; Ramanathan, S.; Thomas, L.; Williams, R. S.; Kumar, S. True random number generation using the spin crossover in $LaCoO_3$. *Nat. Commun.* **2024**, *15*, 4656.

(14) Yang, Z.; Huang, X.; Liu, Y.; Wang, Z.; Zhang, Z.; Ma, B.; Shang, H.; Wang, L.; Zhu, T.; Duan, X.; Hu, H.; Yue, J. Unraveling

the Interplay Between Memristive and Magnetoresistive Behaviors in LaCoO3/SrTiO3 Superlattice-Based Neural Synaptic Devices. *Small Methods* **2025**, *9*, 2401259.
(15) Saitoh, T.; Mizokawa, T.; Fujimori, A.; Abbate, M.; Takeda, Y.; Takano, M. Electronic structure and temperature-induced paramagnetism in $LaCoO_3$. *Phys. Rev. B* **1997**, *55*, 4257−4266.
(16) English, S. R.; Wu, J.; Leighton, C. Thermally excited spin-disorder contribution to the resistivity of $LaCoO_3$. *Phys. Rev. B* **2002**, *65*, 220407.
(17) Izquierdo, M.; Karolak, M.; Prabhakaran, D.; Boothroyd, A. T.; Scherz, A. O.; Lichtenstein, A.; Molodtsov, S. L. Monitoring ultrafast metallization in $LaCoO_3$ with femtosecond soft x-ray spectroscopy. *Communications Physics* **2019**, *2*, 8.
(18) Vogt, T.; Hriljac, J. A.; Hyatt, N. C.; Woodward, P. Pressure-induced intermediate-to-low spin state transition in $LaCoO_3$. *Phys. Rev. B* **2003**, *67*, 140401.
(19) Dudnikov, V. A.; Orlov, Y. S.; Kazak, N. V.; Platunov, M. S.; Ovchinnikov, S. G. Anomalies of the electronic structure and physical properties of rare-earth cobaltites near spin crossover. *JETP Letters* **2016**, *104*, 588−600.
(20) Haas, O.; Struis, R. P. W. J.; McBreen, J. M. Synchrotron X-ray absorption of $LaCoO_3$ perovskite. *J. Solid State Chem.* **2004**, *177*, 1000−1010.
(21) Podlesnyak, A.; Streule, S.; Mesot, J.; Medarde, M.; Pomjakushina, E.; Conder, K.; Tanaka, A.; Haverkort, M. W.; Khomskii, D. I. Spin-State Transition $LaCoO_3$: Direct Neutron Spectroscopic Evidence of Excited Magnetic States. *Phys. Rev. Lett.* **2006**, *97*, 247208.
(22) Feygenson, M.; Novoselov, D.; Pascarelli, S.; Chernikov, R.; Zaharko, O.; Porcher, F.; Karpinsky, D.; Nikitin, A.; Prabhakaran, D.; Sazonov, A.; Sikolenko, V. Manifold of spin states and dynamical temperature effects in $LaCoO_3$: Experimental and theoretical insights. *Phys. Rev. B* **2019**, *100*, 054306.
(23) Karolak, M.; Izquierdo, M.; Molodtsov, S.; Lichtenstein, A. Correlation-Driven Charge and Spin Fluctuations in $LaCoO_3$. *Phys. Rev. Lett.* **2015**, *115*, 046401.
(24) Chakrabarti, B.; Birol, T.; Haule, K. Role of entropy and structural parameters in the spin-state transition of $LaCoO_3$. *Physical Review Materials* **2017**, *1*, 064403.
(25) Klie, R. F.; Zheng, J. C.; Zhu, Y.; Varela, M.; Wu, J.; Leighton, C. Direct Measurement of the Low-Temperature Spin-State Transition in $LaCoO_3$. *Phys. Rev. Lett.* **2007**, *99*, 047203.
(26) Spence, J. C. H. Absorption spectroscopy with sub-angstrom beams: ELS in STEM. *Rep. Prog. Phys.* **2006**, *69*, 725−758.
(27) Krivanek, O. L.; Dellby, N.; Hachtel, J. A.; Idrobo, J. C.; Hotz, M. T.; Plotkin-Swing, B.; Bacon, N. J.; Bleloch, A. L.; Corbin, G. J.; Hoffman, M. V.; Meyer, C. E.; Lovejoy, T. C. Progress in ultrahigh energy resolution EELS. *Ultramicroscopy* **2019**, *203*, 60−67.
(28) Allard, L. F.; Bigelow, W. C.; Jose-Yacaman, M.; Nackashi, D. P.; Damiano, J.; Mick, S. E. A new MEMS-based system for ultra-high-resolution imaging at elevated temperatures. *Microscopy Research and Technique* **2009**, *72*, 208−215.
(29) Sharma, R. *In-Situ Transmission Electron Microscopy Experiments: Design and Practice*, 1st ed.; Wiley, 2023; Chapter 3, pp 77−114.
(30) Radovic, M.; Speakman, S. A.; Allard, L. F.; Payzant, E. A.; Lara-Curzio, E.; Kriven, W. M.; Lloyd, J.; Fegely, L.; Orlovskaya, N. Thermal, mechanical and phase stability of $LaCoO_3$ in reducing and oxidizing environments. *J. Power Sources* **2008**, *184*, 77−83.
(31) Nabatame, T.; Yasuda, T.; Nishizawa, M.; Ikeda, M.; Horikawa, T.; Toriumi, A. Comparative Studies on Oxygen Diffusion Coefficients for Amorphous and -Al2O3 Films using 18O Isotope. *Jpn. J. Appl. Phys.* **2003**, *42*, 7205.
(32) Cai, S.; Dai, J.; Shao, Z.; Rothmann, M. U.; Jia, Y.; Gao, C.; Hao, M.; Pang, S.; Wang, P.; Lau, S. P.; Zhu, K.; Berry, J. J.; Herz, L. M.; Zeng, X. C.; Zhou, Y. Atomically Resolved Electrically Active Intragrain Interfaces in Perovskite Semiconductors. *J. Am. Chem. Soc.* **2022**, *144*, 1910−1920.
(33) Kwon, Y.; An, B.-S.; Moon, J.-Y.; Lee, J.-H.; Yoo, H.; Whang, D.; Yang, C.-W. Control of oxidation behavior in high vacuum transmission electron microscopy. *Mater. Charact.* **2021**, *172*, 110870.
(34) De Groot, F. M. F.; Grioni, M.; Fuggle, J. C.; Ghijsen, J.; Sawatzky, G. A.; Petersen, H. Oxygen 1 *s* x-ray-absorption edges of transition-metal oxides. *Phys. Rev. B* **1989**, *40*, 5715−5723.
(35) Thornton, G.; Tofield, B. C.; Hewat, A. W. A Neutron Diffraction Study of $LaCoO_3$ in the Temperature Range. *J. Solid State Chem.* **1986**, *61*, 301−307.
(36) Jang, J. H.; Kim, Y.-M.; He, Q.; Mishra, R.; Qiao, L.; Biegalski, M. D.; Lupini, A. R.; Pantelides, S. T.; Pennycook, S. J.; Kalinin, S. V.; Borisevich, A. Y. In Situ Observation of Oxygen Vacancy Dynamics and Ordering in the Epitaxial $LaCoO_3$ System. *ACS Nano* **2017**, *11*, 6942−6949.
(37) Hansteen, O. H.; Fjellvag, H.; Hauback, B. C. Crystal structure, thermal and magnetic properties of $La_3Co_3O_8$. Phase relations for $LaCoO_{3-\delta}$ ($0.00 \leq \delta \leq 0.50$) at 673 K. *J. Mater. Chem.* **1998**, *8*, 2081−2088.
(38) Kwon, J.-H.; Choi, W. S.; Kwon, Y.-K.; Jung, R.; Zuo, J.-M.; Lee, H. N.; Kim, M. Nanoscale Spin-State Ordering in $LaCoO_3$ Epitaxial Thin Films. *Chem. Mater.* **2014**, *26*, 2496−2501.
(39) Ma, C.; Lin, N.; Wang, Z.; Zhou, S.; Yu, H.; Lu, J.; Huang, H. Origin of spin-state crossover and electronic reconstruction at the surface of a $LaCoO_3$ nanoparticle. *Phys. Rev. B* **2019**, *99*, 115401.

https://doi.org/10.1021/acs.nanolett.5c03863
Nano Lett. 2025, 25, 16340−16345